Modulation of anti-angiogenic activity using ultrasound-activated nutlin-loaded piezoelectric nanovectors

Materials Today Bio 13 (2022) 100196

Contents lists available at ScienceDirect

Materials Today Bio

journal homepage: www.journals.elsevier.com/materials-today-bio

Modulation of anti-angiogenic activity using ultrasound-activated nutlin-loaded piezoelectric nanovectors

Özlem Şen **, Attilio Marino, Carlotta Pucci, Gianni Ciofani *

Istituto Italiano di Tecnologia, Smart Bio-Interfaces, Viale Rinaldo Piaggio 34, 56025, Pontedera, Italy

ARTICLE INFO

Keywords:
Piezoelectric nanoparticles
Anti-angiogenesis
Invasion
Migration
Nutlin-3a

ABSTRACT

Angiogenesis plays a fundamental role in tumor development, as it is crucial for tumor progression, metastasis development, and invasion. In this view, anti-angiogenic therapy has received considerable attention in several cancer types in order to inhibit tumor vascularization, and the progress of nanotechnology offers opportunities to target and release anti-angiogenic agents in specific diseased areas. In this work, we showed that the angiogenic behavior of human cerebral microvascular endothelial cells can be inhibited by using nutlin-3a-loaded ApoE-functionalized polymeric piezoelectric nanoparticles, which can remotely respond to ultrasound stimulation. The anti-angiogenic effect, derived from the use of chemotherapy and chronic piezoelectric stimulation, leads to disruption of tubular vessel formation, decreased cell migration and invasion, and inhibition of angiogenic growth factors in the presence of migratory cues released by the tumor cells. Overall, the proposed use of remotely activated piezoelectric nanoparticles could provide a promising approach to hinder tumor-induced angiogenesis.

1. Introduction

Angiogenesis is the process referred to the vessel growth, but most usually to a new vessel formation from the already existing vasculature. It plays an essential role in many processes such as embryonic development, ovulation, and wound healing; moreover, it is critical in the progression of many diseases (including arthritis and cancer metastasis) [1,2]. Survival of metastatic cells and thus tumor progression require nutrients and an adequate supply of oxygen; hence, metastatic cells need to stay near blood capillaries for direct contact to the circulatory system [3]. Tumor cells and tumor-associated stromal cells induce an angiogenic switch by the constant secretion of pro-angiogenic factors and stimulate endothelial cell proliferation/migration to generate new blood vessels during cancer progression. In this process, the increased number of endothelial cells leads to form disorganized and immature vessels with disrupted endothelial cell junctions, associated with tumor neo-vessels permeability, fragility, and interstitial fluid pressure [4].

Although tumor angiogenesis is considered a primary therapeutic target, it is also a major challenge in cancer medicine. Conventional therapies focus on the application of anti-angiogenic agents to target and then block the activity of pro-angiogenic factors [5]. Novel approaches envision the combination of anti-angiogenic drugs with chemotherapy or immunotherapy; however, their effectiveness remains a matter of debate [6]. On the other side, nanotechnology offers great tools to target and release anti-angiogenic agents in specific diseased areas [7]. Recently, an innovative approach in cancer nanomedicine has been proposed, depending upon the use of nanomaterials that can remotely respond to external remote stimulation such as ultrasound (US) [8]. In this context, piezoelectric nanomaterials presenting the ability to convert mechanical energy into electricity show interesting potentials in cancer therapy, owing to the non-invasive and wireless delivery of electrical cues able to affect cancer cell fate [9].

In a previous work of ours, a wireless treatment mediated by piezoelectric barium titanate nanoparticles has been used to remotely deliver electric stimulation into breast cancer cells [10]. However, most piezoelectric nanomaterials such as zinc oxide and barium titanate show low biocompatibility and biodegradability [11]. Among piezoelectric polymers, poly(vinylidene fluoride) (PVDF) and PVDF-trifluoro ethylene (P(VDF-TrFE)) are the most studied polymeric piezoelectric materials, because of their biocompatibility and better processability in mild reaction conditions [12]. The literature reports that P(VDF-TrFE)-based scaffolds or films induce cell differentiation and controlled release of drugs upon appropriate US stimulation [13,14]. Furthermore, our recent study showed that P(VDF-TrFE) nanoparticles can be used to inhibit

* Corresponding author.
** Corresponding author.
E-mail addresses: ozlem.sen@iit.it (Ö. Şen), gianni.ciofani@iit.it (G. Ciofani).

https://doi.org/10.1016/j.mtbio.2021.100196
Received 25 October 2021; Received in revised form 21 December 2021; Accepted 24 December 2021
Available online 25 December 2021

cancer progression upon US stimulation by activating anti-proliferation and apoptosis pathways, inducing necrosis, inhibiting cell migration, and decreasing invasion in drug-resistant glioblastoma cells [15].

In the present work, we prepared piezoelectric lipid-polymer nanoparticles owning a core of P(VDF-TrFE) and loaded with nutlin-3a (Nut), being the anti-angiogenic activity of Nut widely reported in the literature [16,17]. The particles were further functionalized with a peptide composed of specific residues of apolipoprotein E (ApoE), that interacts with caveolin-1 protein in endothelial cells [18]. Human cerebral microvascular endothelial cells (hCMEC/D3) were used being widely exploited as a component of blood-brain barrier (BBB) *in vitro* models: they are in fact particularly suitable for the investigation of cellular and molecular mechanisms at the base of many pathologies associated to the central nervous system, including brain cancer [19]. The prepared system was used to modulate the angiogenesis upon US stimulation: *in vitro* studies showed the potential inhibitory effect of the particles on vessel formation, on endothelial cells migration and invasion, and on production of angiogenesis-related cytokines. This study, for the first time in the literature, shows the interaction of piezoelectric nanoparticles with human endothelial cells, and their effect, following mechanical stimulation, on the inhibition of tumor-induced angiogenesis.

2. Experimental Section

2.1. Nanoparticle fabrication and characterization

Nutlin-3a loaded P(VDF-TrFE) nanoparticles (Nut-PNPs) were synthesized and surface-functionalized with a peptide that corresponds to a fragment of apolipoprotein E (ApoE; GenScript), as previously described in a work of our group [15]. Briefly, 2 mL of 5 mg/mL P(VDF-TrFE) (45:65; Piezotech) and 200 μL of 5 mg/mL nutlin-3a (Sigma-Aldrich) in acetone (Sigma-Aldrich) were placed into 4.5 mL of a 1 mg/mL 1, 2-distearoyl-*sn*-glycero-3-phosphoethanolamine-poly(ethylene glycol) (DSPE-PEG; Nanocs) dispersion in water under stirring. The obtained mixture underwent three consecutive cycles of sonication (ultrasonic tip; Fisherbrand™ Q125 Sonicator) and purification (Amicon® centrifuge filters, Ultra-4 Centrifugal Filter Unit, 100 kDa; Sigma-Aldrich) with the pellet suspended in water (4 mL). The polymeric core of the nanoparticles was recrystallized by refluxing (90°C for 60 min) and then by progressively cooling down to 25°C (−1°C/min). Subsequently, 1 mg of DSPE-PEG/DSPE-PEG-maleimide (1:1) was added for the stabilization of the nanoparticle dispersion, which was sonicated for 10 min (ultrasonic tip, 70% amplitude; Fisherbrand™ Q125 Sonicator). Finally, three consecutive centrifugation steps were performed at 15°C (2460 *g* for 15 min; Amicon® centrifuge filters, Ultra-4 Centrifugal Filter Unit, 100 kDa; Sigma-Aldrich) to remove the excess of lipids. The bioconjugation of the nanoparticles with the ApoE peptide was carried out through the maleimide-thiol click reaction [20] by incubating the 141–150 residues of the ApoE (200 μL of a 2 mg/mL water suspension) to 4 mL of the 2 mg/mL nanoparticle dispersion for 4 h at 4°C under shaking. Three centrifugation steps were then carried out as described above to remove the non-bounded peptide. ApoE-PNPs were synthesized following the same protocol used for ApoE-Nut-PNPs, without adding the drug in the polymer/acetone solution. Nut-PNPs and PNPs were obtained skipping the functionalization step. The fluorescent staining of the nanoparticles was obtained by adding 5 μL DiO fluorescent dye (Vybrant™; Invitrogen) to the 2 mL polymer/acetone initial solution.

Morphologic analysis of PNPs, Nut-PNPs, ApoE-PNPs, and ApoE-Nut-PNPs was performed by transmission electron microscopy (TEM) and scanning electron microscopy (SEM). Concerning TEM, a drop of 70 μg/mL nanoparticle dispersions was cast on an ultrathin amorphous carbon film-coated Cu grid composed of 150 mesh and, subsequently, imaging was performed with a JEOL 1011 operating at 100 kV. For SEM imaging, a drop of nanoparticle dispersions was deposited on a silicon wafer. Then, samples were imaged with a Helios NanoLab 600i Dual Beam™ FIB/SEM FEI after gold-sputtering (30 mA for 1 min) with a Quorum Tech Q150RES Gold Sputter Coater. The nanoparticle size was measured from the TEM images by using ImageJ software, and data were reported as average diameter ± standard deviation.

The hydrodynamic size of PNPs, Nut-PNPs, ApoE-PNPs, and ApoE-Nut-PNPs (500 μg/mL) were investigated in water at 37°C by using a Nano Z-Sizer 90 (Malvern Instrument); the ζ-potential measurements were performed in the same conditions. The hydrodynamic size and ζ-potential measurements are shown as the mean ± standard deviation of three different measurements with 10 runs for each of them. CONTIN analysis was used to obtain the intensity distribution, and the value of the hydrodynamic diameter and the polydispersity index (PdI) was assessed by cumulant analysis. Furthermore, stability of PNPs, Nut-PNPs, ApoE-PNPs, and ApoE-Nut-PNPs was assessed at a concentration of 500 μg/mL in plasma obtained from mice blood (see Section 2.4 for details), at 37°C for 14 days, periodically performing dynamic light scattering measurements.

2.2. Cell culture

Human cerebral microvascular endothelial cells (hCMEC/D3; Merck Millipore) were cultured in EndoGRO-MV (Sigma-Aldrich) supplemented with EndoGRO-MV-VEGF Complete Culture Media Kit (SCME003; Sigma-Aldrich), and 1% penicillin-streptomycin (Gibco). T98G cells (ATCC® CRL-1690™) were cultured in Dulbecco's modified Eagle's medium (DMEM; Gibco) supplemented with 10% fetal bovine serum (FBS; Gibco), 1 mM sodium pyruvate (Gibco), 2 mM L-glutamine (Gibco), and 100 IU/mL of penicillin-streptomycin (Gibco). All cell cultures were maintained at 37°C in a 5% CO_2 atmosphere.

2.3. WST-1 assay

For proliferation analysis, hCMEC/D3 cells were seeded at $2{\cdot}10^4$ cells/cm^2 density on Matrigel (10 mg/mL; BD Bioscience) coated 96-well plates and analyzed using WST-1 assay reagent (BioVision) following the manufacturer's instruction. After 24 h from cell seeding, they were incubated with PNPs (100–1000 μg/mL), Nut-PNPs (100–1000 μg/mL), ApoE-PNPs (100–1000 μg/mL), ApoE-Nut-PNPs (100–1000 μg/mL), or Nut (0.2–25 μM) for 72 h. After rinsing the cells with PBS, they were treated with the WST-1 reagent (1:10 dilution in complete EndoGRO-MV media for 45 min at 37°C). The absorbance of the collected supernatants was measured using a microplate reader (Perkin Elmer Victor X3) at 450 nm. The absorbance of blank, corresponding to EndoGRO-MV medium, was subtracted from all measurements. The results were then normalized with respect to the non-treated control culture.

2.4. Hemolysis test

The effect of the nanoparticles on red blood cells (RBCs) integrity was evaluated by a standard hemolysis assay with some modifications [21]. Briefly, blood was collected from mice (discharged samples obtained from animals sacrificed at the end of experimental procedures approved by the ethical committee, authorization 746/2021-PR of the Italian Ministry of Health), and added to a 3.8% sodium citrate solution to prevent coagulation. It was then mixed by gentle inversion of the tube and centrifuged at 1000 *g* for 10 min. The plasma supernatant was removed, and the RBCs were washed 3 times using saline solution (0.9% w/v). The final suspension consisting of 5% (v/v) RBCs was obtained by adding saline solution. 500 μg/mL of PNPs, Nut-PNPs, ApoE-PNPs, or ApoE-Nut-PNPs were added in 5% (v/v) RBC suspension and incubated for 72 h at 37°C by gently shaking on an orbital plate shaker. The positive control (C+) consisted of 50% (v/v) deionized water, while the negative control (C-) consisted of 6% (v/v) PBS solution in RBC suspension (5% v/v). After incubation, the tubes were centrifuged at 500 *g* for 5 min. The absorbance of hemoglobin released into the supernatants was determined using a microplate reader at 540 nm. 6% (v/v) PBS solution and 50% (v/v) deionized water were used as negative (0% hemolysis) and

positive controls (100% hemolysis), respectively. The percentage of hemolysis was calculated normalizing all experimental results to the mean absorbance value, which represents 100% hemolysis in positive control.

2.5. Cellular internalization

Cells were seeded at $2{\cdot}10^4$ cells/cm^2 in μ-Dishes (35 mm; Ibidi) coated with Matrigel (10 mg/mL) for confocal microscopy imaging. After 24 h, cultures were incubated with 500 μg/mL of DiO-labelled PNPs, Nut-PNPs, ApoE-PNPs, or ApoE-Nut-PNPs for further 24 and 72 h. Then, the cells were fixed using 4% paraformaldehyde (PFA; Sigma-Aldrich) at 4°C for 20 min. Next, they were rinsed three times with PBS. hCMEC/D3 cells were incubated with TRITC-phalloidin (1:200 v/v; Sigma-Aldrich) and Hoechst (1:1000 v/v; Invitrogen) at 37°C for 45 min for the imaging of nuclei and *f*-actin, respectively. Finally, a confocal fluorescence microscope (C2 system Nikon) was used to acquire 2D images and 3D rendering.

2.6. In vitro tube formation assay

Tube formation assay was carried out by growing hCMEC/D3 cells on Matrigel-coated wells. A 24-well plate was coated with Matrigel (10 mg/mL), allowed to solidify at 37°C for 30 min. Cell cultures were divided in 8 groups including controls w/o (Control) or w/ (Control + US) US stimulation, cells treated with free Nut w/o (Nut) or w/ (Nut + US) US stimulation, cells treated with ApoE-PNPs w/o (ApoE-PNPs) or w/ (ApoE-PNPs + US) US stimulation, and cells treated with ApoE-Nut-PNPs w/o (ApoE-Nut-PNPs) or w/ (ApoE-Nut-PNPs + US) US stimulation. To assess the particle effect on the tube formation, cells ($2{\cdot}10^4$ cells/cm^2) were treated for 24 h with Nut 21.5 μM (corresponding to Nut loaded in 500 μg/mL of ApoE-Nut-PNPs), ApoE-PNPs (500 μg/mL), or ApoE-Nut-PNPs (500 μg/mL). A previously described protocol was followed for chronic US stimulation [15]. Briefly, the US was delivered at 1 MHz frequency and 1 W/cm^2 intensity. Single stimuli lasted 200 ms each and were activated every 2 s. US were applied for 1 h *per* day for 2 days. This treatment protocol was applied since it activates piezoelectricity without affecting cell behavior/proliferation, and it does not induce any detectable increment in the temperature of cell media [22]. At the end of the stimulation, images were acquired with a bright-field microscope (Eclipse Ti, Nikon). The number of junctions, the total branching length, and the total mesh area were calculated with ImageJ software using the "Angiogenesis" plug-in, following a previously described protocol [23].

2.7. Migration and invasion assays

Before transwell insert experiments, $2{\cdot}10^4$ cells/cm^2 of T98G cells were grown in EndoGRO-MV media for 2 days to obtain conditioned medium. The obtained conditioned medium was sterilized by filtration through a 0.2 μm filter (Sartorius Minisart Plus Syringe Filters) before use.

For migration analysis, in a separate 24-well plate, hCMEC/D3 ($2{\cdot}10^4$ cells/cm^2) cells were mixed with plain medium (as control), Nut (21.5 μM), ApoE-PNPs (500 μg/mL) or ApoE-Nut-PNPs (500 μg/mL), seeded on 6.5 mm transwell inserts with a pore size 8 μm (Costar), and let them attach to the inserts overnight. The following day, the transwell inserts were transferred to the plate containing T98G cells. US stimulation was applied as described in Section 2.5. Cells were co-cultured to allow the cancer cells to induce the hCMEC/D3 migration. Following the US stimulation, cells were fixed with 4% (w/v) PFA as described above and washed three times with PBS. The non-migrated hCMEC/D3 cells were removed from the top chamber of the insert using a cotton swab. The migrated hCMEC/D3 cells on the lower chamber of the insert were permeabilized using 0.1% (v/v) Triton X-100 (Sigma-Aldrich) and then stained using Hoechst (1:1000 v/v) at 37°C for 45 min. The migrated cells were imaged by using an Eclipse Ti fluorescence microscope (Nikon) and counted with ImageJ software.

The invasion capability of endothelial cells was assessed using the Invasion Assay Kit (ab235887; Abcam) following the manufacturer's protocol but with some modifications. The upper chamber of the inserts was coated using Matrigel (0.5 mg/mL) to form a thin film. After film formation, hCMEC/D3 cells were seeded as described for the migration assay; however, in the bottom chamber, only the conditioned media were used as invasion-inducer. The US stimulation was performed with the same parameters described above. The non-invaded cells on the top chamber were detached using a cotton swab, and cell dye (1:250 v/v in PBS) was added into the lower chamber for 30 min. Next, fluorescence was read ($\lambda_{ex} = 485$ nm; $\lambda_{em} = 530$ nm) using a plate reader. Finally, the fluorescence was converted into cell numbers using a standard calibration curve as depicted in Fig. S1A.

2.8. 3D spheroid invasion assay

The hCMEC/D3 cell invasion was further investigated by a 3D spheroid invasion assay using a previously described method but with some modifications [24]. Prior to the 3D spheroid invasion assay, a non-adherent plate was prepared by using 2% (w/v) agarose (Sigma-Aldrich). The agarose-coated wells were thereafter sterilized applying UV for 30 min. The invasion matrix was prepared by using Matrigel (10 mg/mL), and the conditioned medium was collected from T98G cultures ($2{\cdot}10^4$ cells/cm^2), which were kept in EndoGRO-MV for 2 days. hCMEC/D3 cells ($55{\cdot}10^3$ cells/well) were added to a non-adherent 48-well plate and incubated for 48 h. The growth medium was removed after the formation of spheroids, and at this point plain medium (as control), Nut (21.5 μM), ApoE-PNPs (500 μg/mL), or ApoE-Nut-PNPs (500 μg/mL) were added into the wells for a further 24 h. Then, the treatment media were removed, and the spheroids were harvested. They were then transferred to the matrix-coated wells, and the conditioned media induced the invasion. The US stimulation was performed using the same parameters described above; the invaded cells were imaged with bright-field microscopy at 0 and 48 h from the start of invasion induction, and images were then analyzed using ImageJ software.

2.9. Cytokines release assessment

hCMEC/D3 cells ($2{\cdot}10^4$ cells/cm^2) were incubated with plain medium (as control), Nut (21.5 μM), ApoE-PNPs (500 μg/mL), or ApoE-Nut-PNPs (500 μg/mL) for 24 h on Matrigel-coated wells. After incubation, cultures were stimulated with US as previously described (1 h *per* day for 2 days). The supernatants were then collected and centrifuged at 1000 *g* for 10 min for the elimination of any cellular debris. In order to profile angiogenesis-related cytokines, *i.e.*, tumor necrosis factor-alpha (TNF-α), insulin-like growth factor-1 (IGF-1), vascular endothelial growth factor (VEGF), interleukin-6 (IL-6), basic fibroblast growth factor (FGFb), transforming growth factor beta (TGFb), epidermal growth factor (EGF), and leptin, human angiogenesis ELISA strip I (Signosis) was performed following the manufacturer's protocol, by exploiting standard calibration curves (Fig. S1B) and normalizing the values with respect to the total protein content *per* sample. For protein extraction, RIPA buffer (Sigma-Aldrich) and protease inhibitor (1:1000 v/v, Sigma-Aldrich) were used to lyse the cells. Finally, the bicinchoninic acid assay (BCA; Sigma-Aldrich) was used to measure the protein content, according to the manufacturer's protocol.

2.10. Statistical analysis

Statistical analysis was carried out using analysis of variance (ANOVA) followed by Fisher's *post-hoc* test; data are presented as mean value ± standard deviation of three independent experiments. The significance was set at $p < 0.05$.

3. Results

3.1. Nanoparticle characterization

The characterization of PNPs, Nut-PNPs, ApoE-PNPs, and ApoE-Nut-PNPs is reported in Fig. 1 and Fig. S2. Representative TEM and SEM images of ApoE-PNPs (Fig. 1A and C), ApoE-Nut-PNPs (Fig. 1B and D), PNPs (Fig. S2A and Fig. S2C), and Nut-PNPs (Figs. S2B and S2D) suggest the presence of spherical-shaped nanoparticles. The size of the PNPs, Nut-PNPs, ApoE-PNPs, and ApoE-Nut-PNPs, estimated through image analysis, resulted to be respectively 62 ± 20 nm, 56 ± 12 nm, 66 ± 22 nm, and 76 ± 16 nm. The hydrodynamic diameters of PNPs, Nut-PNPs, ApoE-PNPs, and ApoE-Nut-PNPs in water resulted instead to be respectively 212 ± 10 nm, 266 ± 5 nm, 267 ± 2 nm, and 203 ± 2 nm (Fig. 1E and Fig. S2E), with a PDI of 0.32 ± 0.08, 0.30 ± 0.09, 0.33 ± 0.05, and 0.18 ± 0.01: as expected, these values are slightly higher than the particle size determined with electron microscopy due to the presence of the hydration shell. The ζ-potential of PNPs, Nut-PNPs, ApoE-PNPs, and ApoE-Nut-PNPs resulted −20.8 ± 0.9 mV, −18.4 ± 0.8 mV, −21.6 ± 0.7 mV, and −18.3 ± 0.6 mV, respectively (Fig. 1F and Fig. S2F). The stability of PNPs, Nut-PNPs, ApoE-PNPs, and ApoE-Nut-PNPs was monitored using DLS measurements up to 14 days (Fig. 1G and Fig. S2G), and results showed as the hydrodynamic diameter of the particles gradually increase after 3 days, most probably because of protein corona formation, as suggested by the literature [25].

Overall, we can conclude that neither the surface functionalization or the drug loading significantly changed size, ζ-potential, or stability of nanoparticles.

Concerning drug loading and release, in a previous study, we reported that nutlin-3a loaded in ApoE-PNPs was found to be 2.5 ± 0.7 wt%, while the release of drug was 12.5 ± 0.3% at pH 4.5 after 48 h upon ultrasound stimulation [15].

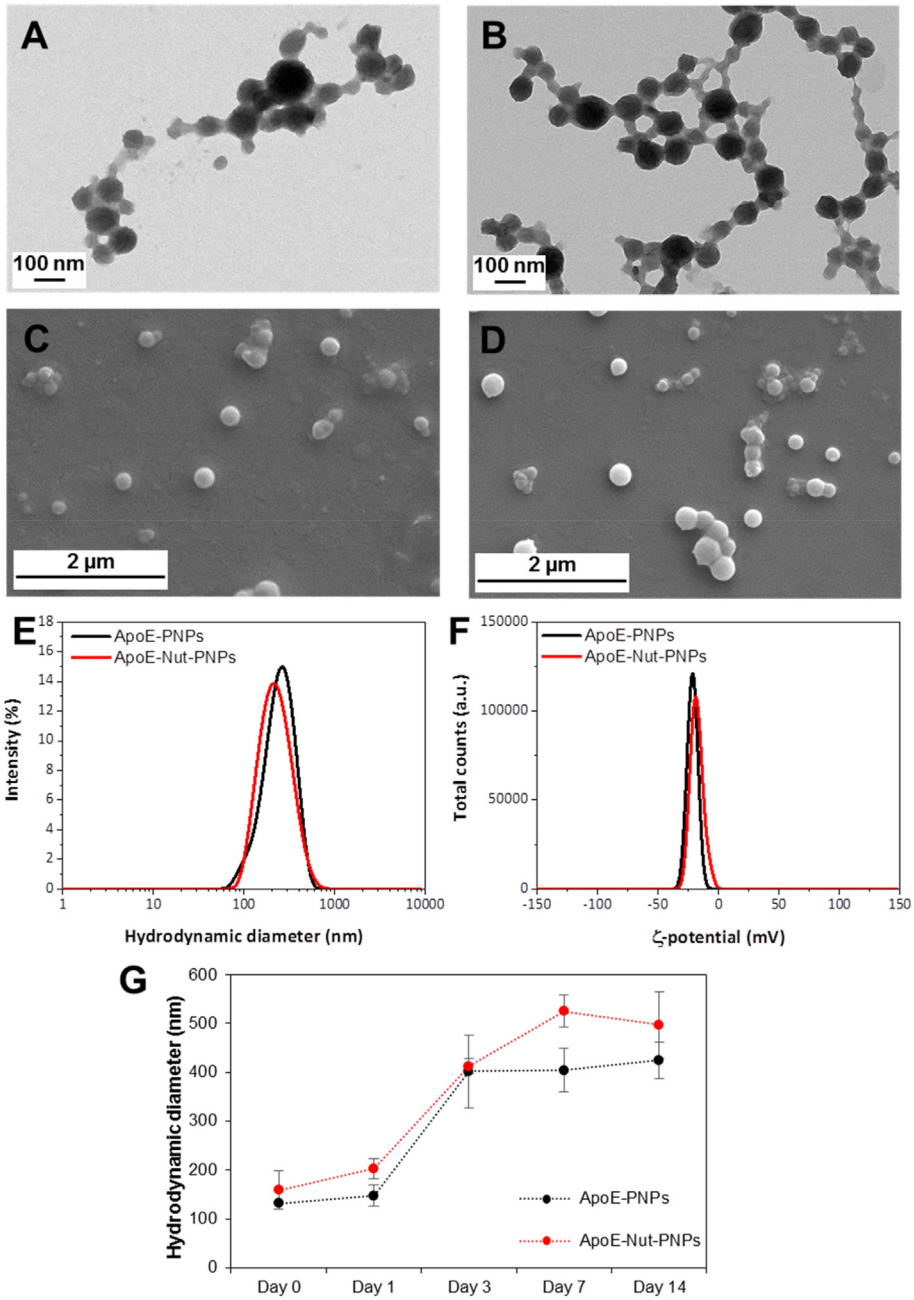

Fig. 1. Nanoparticle characterization. Representative TEM images of **A)** ApoE-PNPs and **B)** ApoE-Nut-PNPs; representative SEM images of **C)** ApoE-PNPs and **D)** ApoE-Nut-PNPs; **E)** intensity distribution (%) as a function of the hydrodynamic diameter (nm) of ApoE-PNPs (black) and ApoE-Nut-PNPs (red); **F)** ζ-potential (mV) distribution of ApoE-PNPs (black) and ApoE-Nut-PNPs (red); **G)** stability study of the particles in plasma up to 14 days (ApoE-PNPs in black and ApoE-Nut-PNPs in red). (For interpretation of the references to color in this figure legend, the reader is referred to the Web version of this article.)

3.2. Biocompatibility assessment

The cytocompatibility of the nanoparticles and of the free drug was assessed *in vitro* on human endothelial cells using WST-1 colorimetric assay. There is no significant effect on cell culture metabolism of hCMEC/D3 cells treated with 0.2–25 μM of free Nut (Fig. S3, $p > 0.05$), 100–1000 μg/mL of PNPs, 100–1000 μg/mL of Nut-PNPs, 100–1000 μg/mL of ApoE-PNPs, or 100–1000 μg/mL of ApoE-Nut-PNPs (Fig. 2A, $p > 0.05$), suggesting the biocompatibility and the safety of the nanoparticles. Following experiments were carried out by using a safe concentration of 500 μg/mL of nanoparticles, and the corresponding concentration of Nut 21.5 μM (for comparison with drug-loaded nanoparticles).

We tested hemolytic activity in order to preliminarily determine whether nanoparticles present any issue that could prevent their interaction with blood, and thus their safety for clinical translation. As depicted in the inlet of Fig. 2B, showing a representative photo of the hemolysis test, the supernatant of the positive control (C+) was completely red and transparent, demonstrating a complete disruption of RBC membranes. Conversely, supernatants following nanoparticle treatment suggest no significant hemolysis, being colorless like the negative control (C-). The quantitative assessment (Fig. 2B) confirmed no significant hemolytic phenomena, being the hemolysis percentage 0.8 ± 0.8%, 1.2 ± 0.4%, 0.4 ± 0.2%, and 0.4 ± 0.4% for PNPs, Nut-PNPs, ApoE-PNPs, and ApoE-Nut-PNPs, respectively ($p > 0.05$), suggesting the safety of the nanoparticles at the tested concentration.

3.3. Nanoparticle/cell interaction

Upon treatment with DiO-labelled Nut-PNPs or ApoE-Nut-PNPs, the cellular localization of the nanoparticles was qualitatively assessed by using confocal microscopy after 24 and 72 h of incubation (Fig. 3). Representative confocal microscopy images of fluorescently labelled nanoparticles in green, *f*-actin in red, and nuclei in blue are reported as 2D images and 3D rendering, showing nanoparticles associated with the hCMEC/D3 tubes at 24 h (Figs. 3A) and 72 h (Fig. 3B). Samples incubated with ApoE-Nut-PNPs showed a remarkable time-dependent increase of nanoparticles interfaced to tubes. In general, a higher nanoparticle signal can be observed in cultures treated with ApoE-Nut-PNPs with respect to those ones incubated with non-functionalized Nut-PNPs, at both time points, suggesting the effectiveness of the functionalization in promoting nanoparticle-cell interaction. The same trend can be observed for non-loaded PNPs and ApoE-PNPs (Fig. S4).

3.4. In vitro tube formation

Although angiogenesis is a complex process occurring during cancer progression, tube formation is considered one of its key steps. *In vitro* endothelial tube formation assay was carried out on hCMEC/D3 cells by

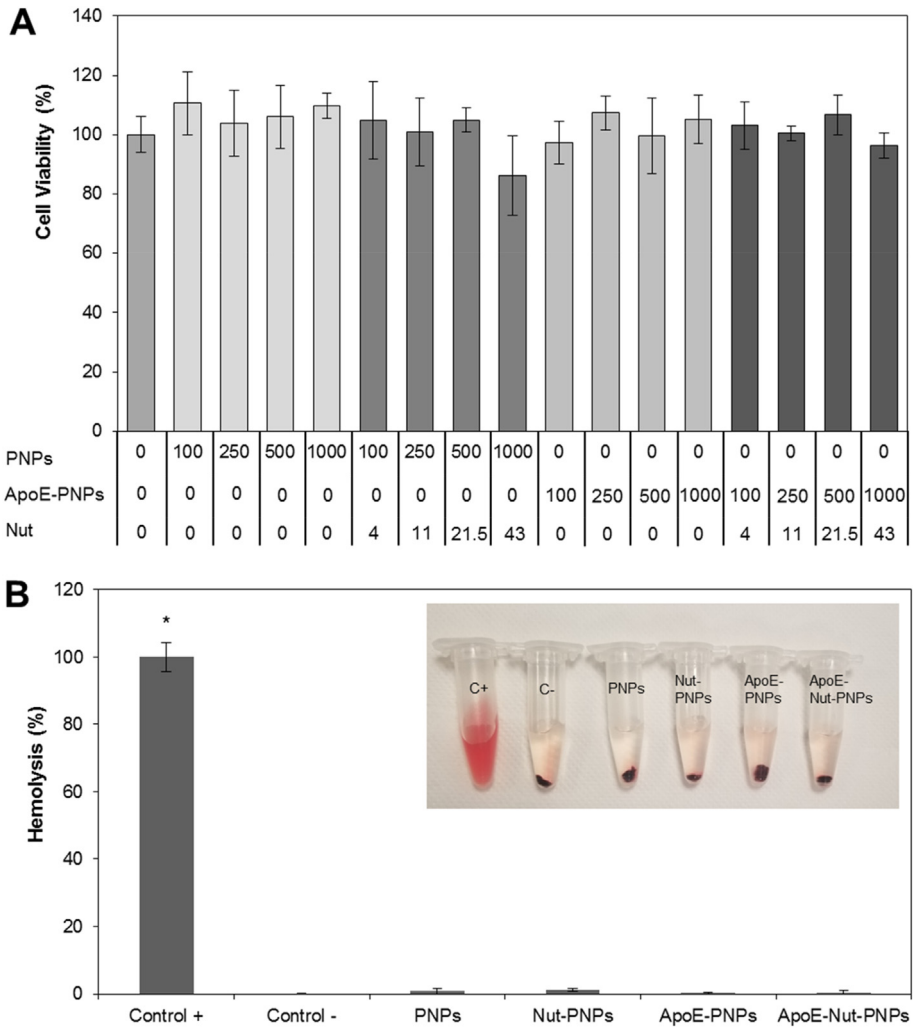

Fig. 2. Biocompatibility evaluation of PNPs, Nut-PNPs, ApoE-PNPs, and ApoE-Nut-PNPs. **A)** Cell viability assessment of the nanoparticles on hCMEC/D3 cells by using WST-1 assay; **B)** *in vitro* hemolysis assay results, where C+ represents the positive control and C- the negative control (*$p < 0.05$). In the inlet, a representative photo of the test is reported.

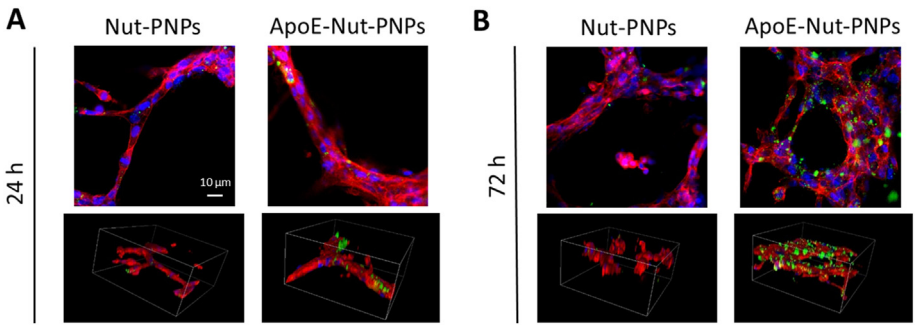

Fig. 3. Internalization of DiO-stained Nut-PNPs and ApoE-Nut-PNPs (nanoparticles in green, *f*-actin in red, nuclei in blue). Representative single *z*-stack confocal images (top) and 3D confocal rendering (bottom) of hCMEC/D3 cells at **A)** 24 h and **B)** 72 h of incubation. For 3D rendering, scan area size is $x = 212$ μm, $y = 212$ μm, $z = 110$ μm. (For interpretation of the references to color in this figure legend, the reader is referred to the Web version of this article.)

considering 8 experimental groups to investigate the potential inhibitory effects of particles on vessel formation in the presence or absence of US stimulation. Endothelial cells were mixed with the nanoparticles, cultured on Matrigel matrix for differentiation and formation of tube-like structures, and visualized using bright-field microscopy imaging (Fig. 4A). The qualitative assessment of the tube formation shows the stunted growth of the vessels in ApoE-Nut-PNPs + US stimulated cultures; however, the tubular vessels matured in all other experimental classes. The ability of hCMEC/D3 cells to form tubular vessels was also quantitatively assessed by calculating the number of junctions, the total branching length, and the total mesh area as shown in Fig. 4B, C, and 4D, respectively. In good agreement with bright-field microscopy images, the analysis of ApoE-Nut-PNPs + US stimulated cultures showed a significant reduction in their length, junctions, and mesh area. The number of junctions significantly decreased to 191 ± 3 ($p < 0.05$) in ApoE-Nut-PNPs + US stimulated cultures compared to control cultures (276 ± 25 for Control; 252 ± 23 for Control + US). A similar trend for ApoE-Nut-PNPs + US treated cells was observed in total branching: the length was significantly reduced to 12,077 ± 125 μm ($p < 0.05$) compared to the Control (14,653 ± 666 μm) and the Control + US (13,802 ± 780 μm) cultures. In addition, ApoE-Nut-PNPs + US stimulated cultures showed a significant decrease in total mesh area (231,463 ± 28,310 μm^2, $p < 0.05$), while the total mesh areas were 409,784 ± 43,501 μm^2 and 420,827 ± 27,252 μm^2 for Control and Control + US cultures, respectively. The results show the significant role of ApoE-Nut-PNPs in deforming the vessel formation in the presence of piezoelectric stimulation.

3.5. Transwell insert migration and invasion assays

In tumor angiogenesis, endothelial cell migration occurs towards the migratory cues that are released by the tumor cells: this considered, the migration and invasion ability of hCMEC/D3 cells were tested using transwell inserts for all the 8 previously mentioned experimental classes in the presence of the conditioned media obtained from T98G cancer cells. Fig. 5A depicts the representative images of migrated cells, showing a few cells migrated through the transwell insert upon ApoE-Nut-PNPs + US stimulation. In line with this qualitative observation, upon quantitative evaluation, a significant decrease in the number of migrated cells was found in cultures treated with ApoE-Nut-PNPs + US (13 ± 2 cells, $p < 0.05$) compared to the control cultures (63 ± 10 cells for Control; 75 ± 11 cells for Control + US), as well as with respect to the other 8 experimental classes (68 ± 13 cells for Nut; 63 ± 10 cells for ApoE-PNPs; 58 ± 10 cells for ApoE-Nut-PNPs; 54 ± 8 cells for Nut + US, 74 ± 8 cells for ApoE-PNPs + US), as shown in Fig. 5B.

In agreement with migration assay results, the number of invaded cells that crossed the Matrigel in the ApoE-Nut-PNPs + US stimulation was significantly decreased to 2441 ± 652 cells ($p < 0.05$) with respect to Control (10147 ± 463 cells), Nut (10578 ± 1480 cells), ApoE-PNPs (10311 ± 536 cells), ApoE-Nut-PNPs (9377 ± 474 cells), Control + US (8828 ± 1625 cells), and Nut + US (9814 ± 1289 cells), as reported in Fig. 5C. Additionally, a significant decrease in the number of cells undergoing invasion was found upon ApoE-PNPs + US treatment (3991 ± 483 cells, $p < 0.05$) with respect to control cultures.

3.6. 3D spheroid invasion assay

We further evaluated the inhibitory effect of Nut, ApoE-PNPs, and ApoE-Nut-PNPs on endothelial cells invasion capability using the 3D spheroid invasion assay, where particles-treated hCMEC/D3 spheroids have been embedded in basement matrix including Matrigel. The representative images of spheroids for all the experimental conditions are shown in Fig. 6A. The images show that Control, Control + US, Nut, Nut + US, ApoE-PNPs, and ApoE-Nut-PNPs cultures break the extracellular matrix (ECM) confinement and invade out of the spheroids after 48 h; however, ApoE-PNPs + US and ApoE-Nut-PNPs + US cultures show a few cells undergoing invasion out of the spheroids, in agreement with the transwell insert invasion assay. The whole area of ApoE-PNPs + US and ApoE-Nut-PNPs + US treated spheroids significantly decreased to 138207 ± 38052 μm^2 and 130067 ± 31247 μm^2, respectively ($p < 0.05$ with respect to the other experimental classes), being instead the whole spheroid area 300683 ± 12834 μm^2 for Control and 249119 ± 45842 μm^2 for Control + US, as reported in Fig. 6B. These data confirm that ApoE-PNPs- and ApoE-Nut-PNPs-mediated piezoelectric stimulation inhibits cell invasion, an important step in tumor angiogenesis.

3.7. Investigation of angiogenesis-related cytokines

Secretion of angiogenesis-related cytokines has been evaluated for all the 8 considered experimental classes as shown in Fig. 7 and Fig. S5. A significant reduction ($p < 0.05$) was observed concerning IL-6 and FGFb in ApoE-Nut-PNPs + US treated cultures. The release of IL-6 was strongly decreased to 32.0 ± 0.1 pg/μg ($p < 0.05$) with respect to the controls (Control = 59.3 ± 4.4 pg/μg; Control + US = 59.3 ± 6.8 pg/μg), as well as in comparison to all the other 8 experimental conditions. Furthermore, IL-6 levels were significantly reduced to 39.7 ± 4.7 pg/μg in ApoE-PNPs + US treatment in comparison to the control cultures. Concerning FGFb levels, a significant reduction was observed just in the ApoE-Nut-PNPs + US treated cultures (61.5 ± 2.1 pg/μg) compared to the Control (100.7 ± 10.9 pg/μg). Concerning the other investigated cytokines (IGF-1, EGF, VEGF, TGFb, TNFa, and leptin), no significant differences were found among all the 8 experimental classes (Fig. S5).

4. Discussion

Cancer cells require a constant supply of nutrients and oxygen, together with the removal of waste materials, because of their high metabolic rate. In this context, angiogenesis plays a fundamental role in tumor progression; moreover, apart from serving as nutrient and waste

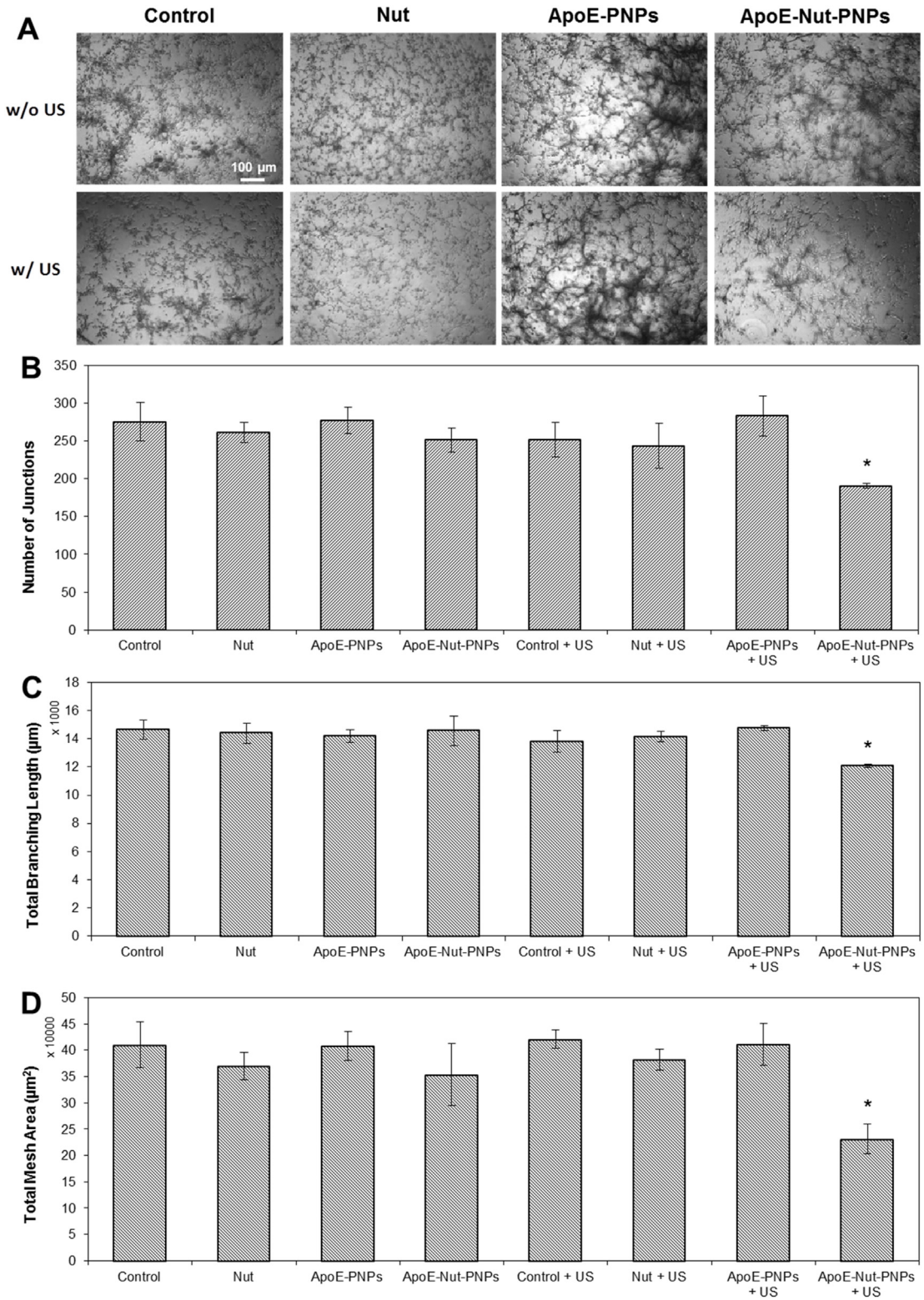

Fig. 4. Tube formation assay. **A)** Representative images of endothelial cells on Matrigel-coated plate during *in vitro* tube formation assay ($t = 48$ h); quantification of **B)** the number of junctions, **C)** the total branching length, and **D)** the total mesh area (*$p < 0.05$).

transporter, it also facilitates the dissemination of cancer cells to distant sites, leading to metastasis [26]: inhibiting angiogenesis is thus a promising methodology to hinder cancer progression.

Among numerous types of therapeutic strategies (such as combining anti-angiogenic drugs with chemotherapy or immunotherapy), the nanotechnology-based approach has emerged as a new treatment strategy in tumor-associated angiogenesis [27]. Nanoparticles can be used as effective tools owing to several advantages over plain drugs, providing high payloads of the therapeutic agents along with reduced toxicity and increased half-life, besides selective targeting thanks to the easy tailoring of the particle surface. In addition, these features might be used for fine-tuning the pharmacological profile of the drugs [28].

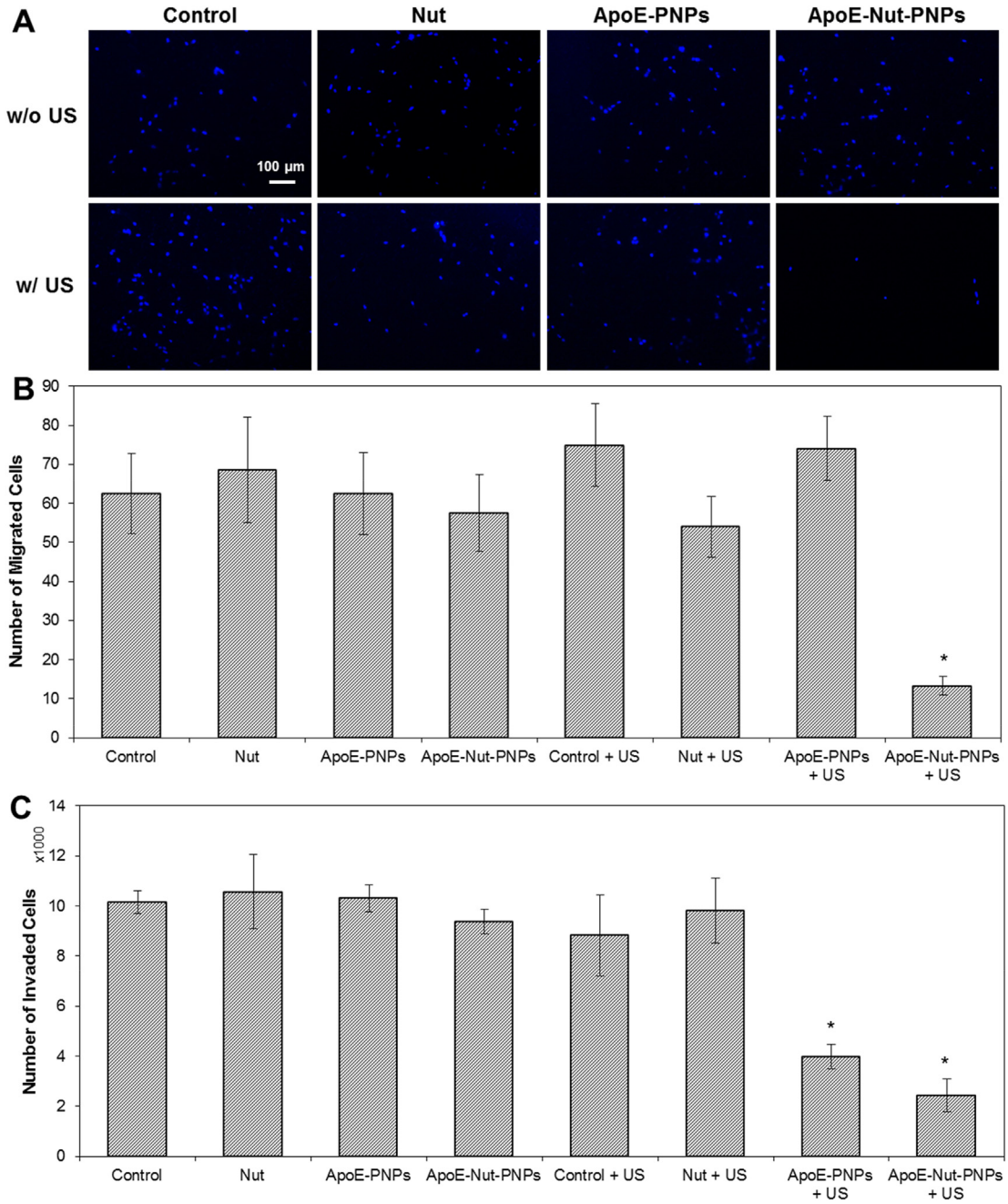

Fig. 5. Migration and invasion assays **A)** Representative fluorescence images of endothelial cell nuclei (in blue) and **B)** quantification of the number of migrated cells during the transwell membrane migration assay ($t = 48$ h); **C)** number of hCMEC/D3 cells that underwent invasion through the Matrigel-coated filter (*$p < 0.05$). (For interpretation of the references to color in this figure legend, the reader is referred to the Web version of this article.)

In this context, the present study was designed to assess the anti-angiogenic properties of ApoE-Nut-PNPs upon US stimulation. The particles showed monodisperse distribution and negative ζ-potential value, which is typically characterized by higher biocompatibility and a slower cell uptake rate compared to nanomaterials with positive ζ-potential values [29], while ApoE functionalization enhances the interaction with hCMEC/D3 cells [30]. ApoE binds to the low-density lipoprotein (LDL) receptors, which are overexpressed in brain endothelial cells [31]. ApoE coating was reported to enhance particle crossing through the BBB by transcytosis [32], and indeed our previous study showed an increment (about 20%) of ApoE-coated PNPs crossing an *in vitro* BBB model, with respect to non-functionalized PNPs [15]. Another group also showed an about 2-fold increment of cellular uptake of ApoE-functionalized solid lipid particles, suggesting the BBB crossing *via* a transcellular pathway [33]. In the present work, an increased hCMEC/D3 tube targeting efficacy was found to be associated with ApoE functionalization, independent from Nut loading. These results are in line with the literature, where nanoparticle functionalization with ApoE is exploited to enhance the BBB targeting *via* LDL receptor recognition. The increased incubation time increases the probability of ApoE binding to the LDL receptor of the brain microvascular endothelial cells, and, consequently, enhances nanoparticle accumulation at tube level [34].

In tumor angiogenesis, the endothelial cells from the already existing vasculature spread for the formation of new blood vessels toward the direction of the tumor [35]. To observe this phenomenon, we cultured hCMEC/D3 cells together with particles on Matrigel matrix to show the potential inhibitory effect of the particles on vessel formation. The result of *in vitro* tube formation assay shows that ApoE-Nut-PNPs + US

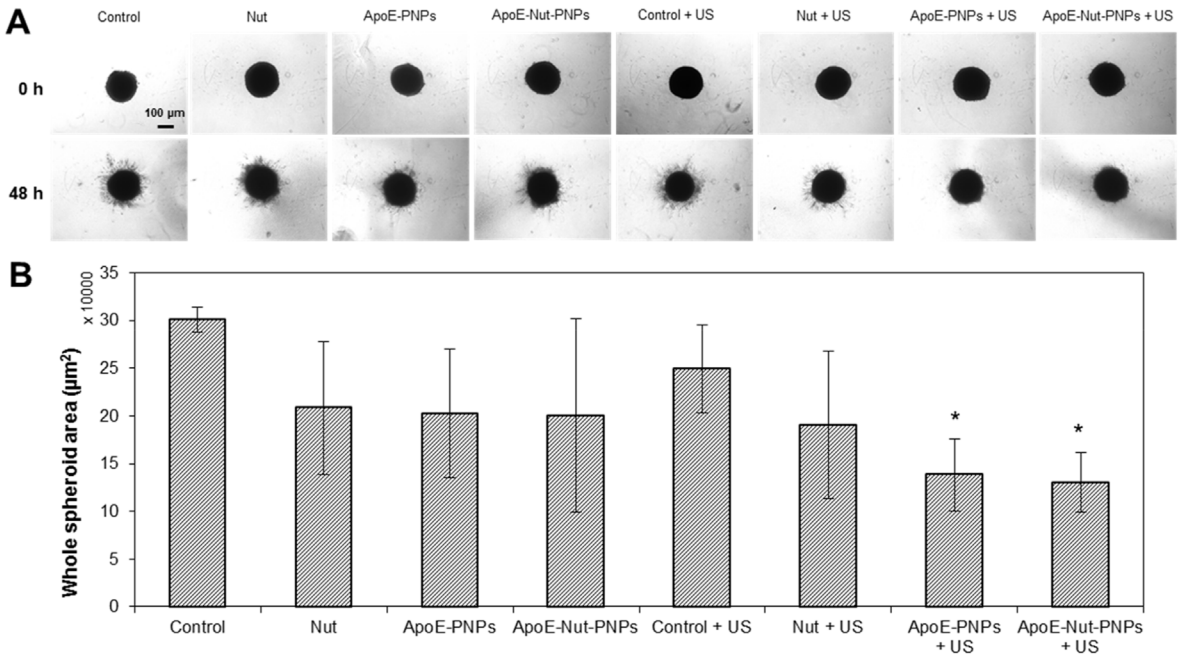

Fig. 6. 3D invasion assay. **A)** Representative images of 3D spheroid invasion assay showing cell spreading out from the spheroids into the Matrigel matrix; **B)** quantification of the whole spheroids area (*$p < 0.05$).

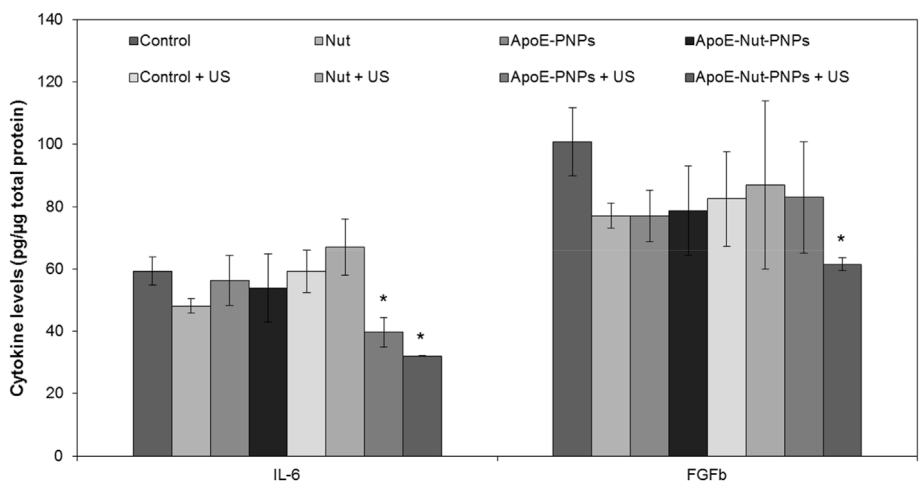

Fig. 7. Investigation of angiogenesis-related cytokines released from hCMEC/D3 cells upon different treatments. Cytokine levels have been normalized according to the total protein content of each sample (*$p < 0.05$).

treatment disrupts the capillary tube formation *in vitro* at a non-toxic concentration (500 μg/mL) by decreasing the number of junctions, the total branching length, and the total mesh area, features that are considered to be critical for angiogenesis process [36]. The ability of ApoE-Nut-PNPs to suppress capillary tube formation could not be ascribed to a generalized cytotoxic effect, since the tested concentration does not affect cell viability. The effects of nutlin-3a on inhibiting vessel formation appeared to be ascribable to the upregulation of the p53 pathway and to apoptosis induction in human umbilical vein endothelial cells (HUVECs) [37]. Another study also shows that nutlin-3a suppresses either the tube growth and decreases the number of capillary connections in HUVECs by upregulating the p53 target genes *MDM2*, cyclin-dependent kinase inhibitor 1A p21 (*CDKN1A/p21)*, and growth/differentiation factor-15 (*GDF-15)*, along by inhibiting cell cycle progression [38]. Additionally, Su *et al.* found that low-intensity pulsed US inhibits *in vitro* tube formation of human endothelial cells *via* p38 mitogen-activated protein kinase (MAPK)-mediated activation of the endoplasmic reticulum stress response [39]. Although Nut is known to inhibit the vessel formations, we did not indeed observe any effect of the plain drug in our study; conversely, the piezoelectric stimulation enhanced the chemotherapeutic efficacy of Nut, in line with the literature [40].

Endothelial cell migration is one of the key steps of angiogenesis [41]; here, we performed a transwell insert migration assay, where particles-treated hCMEC/D3 cells were grown on the top chamber of the transwell membrane and migrated against the migratory cues secreted by cancer cells (T98G glioblastoma multiforme [42]). During the 48 h co-culture period, a few ApoE-Nut-PNPs + US treated endothelial cells migrated through the bottom chamber with respect to the other experimental classes. The literature reports as nutlin-3 treatment significantly decreases the migration of HUVECs co-cultured with lymph node carcinoma of the prostate (LNCaP) cells through up-regulation of *TNF-α*, matrix metallopeptidase 9 (*MMP9)*, and C-X-C motif chemokine ligand 10 (*CXCL10)* [43]. Considering physical cues, it is worth mentioning the

effects of low-frequency magnetic fields, that were found to reduce the number of migrated HUVECs by causing an increment of cells in the G2/M phase of the cell cycle [44].

Cancer cell migration is intertwined with the invasion process, where cells should adhere to the ECM, degrade the basement membrane matrix, and infiltrate the ECM through a 3D process [45]. Here, the invasion ability of particles-treated endothelial cells *via* Matrigel-coated transwell membrane was tested against the migratory cues released by cancer cells. The number of invaded cells in ApoE-Nut-PNPs + US and ApoE-PNPs + US treated cultures was significantly reduced with respect to the control cultures, although no significant differences were found in the transwell insert migration assay. This may be due to the different mechanisms underlying migration and invasion processes, where invasion refers to the ability of cells to travel through the ECM within a tissue or to infiltrate into neighboring tissues, while cell migration is the directed movement of cells in response to a chemical or mechanical cue [46,47]. It was reported that nutlin-3 effectively inhibited HUVEC invasion in an MCF-7 (breast cancer cell line)-HUVEC co-culture system by activating Ras homolog family member A (RhoA) under hypoxic conditions [48]. In another study, nutlin-3 leads to inhibition of invasion and migration in gemcitabine-resistant hepatocellular carcinoma cells, leading to an increase of the expression of E-cadherin and a downregulation of the expression of vimentin, Snail, and Slug [49]. Weitz *et al.* instead showed that low-intensity focused US initiates a calcium wave *via* siRNA-mediated downregulation of both inositol trisphosphate receptors and transient receptor potential channels in invasive prostate (PC-3 and DU-145) and bladder (T24/83) cancer cell lines, leading to invasion inhibition [50].

To further evaluate endothelial cell invasion, a 3D spheroid invasion assay was carried out using particles-treated hCMEC/D3 cells on Matrigel basement matrix in the presence of cancer cell migration cues. The results showed a fewer number of cells undergoing invasion out of the spheroids in ApoE-Nut-PNPs + US and ApoE-PNPs + US treated cultures, which is in line with the transwell invasion assay. Literature reports as high-frequency ultrasound stimulation elicits cytosolic calcium waves in MDA-MB-231 cells, resulting in lower invasiveness [51]. In this study, low frequency (1 MHz) was used, thus no significant effects were observed in absence of piezoelectric nanoparticles; moreover, the fact that no significant differences between ApoE-PNPs + US and ApoE--Nut-PNPs + US treated spheroids were detected suggests that 3D invasion inhibition is mainly due to the electric stimulation rather than to an effect of the drug. Another study showed that treatment with alternating electric fields inhibits the metastatic potential of U87 and U373 glioblastoma cells *via* the nuclear factor kappa B (NF-kB), MAPK, and PI3K/AKT signaling pathways, and suppresses angiogenesis of HUVECs by downregulating VEGF, hypoxia-inducible factor 1-alpha (HIF1-α), MMP2, and MMP9 [52]. In our study, data suggest that piezoelectric stimulation enhances the inhibition of tumor-induced endothelial cell migration and invasion.

Angiogenesis is strictly associated with inflammatory processes in terms of supplying nutrients together with the removal of waste material to preserve physiological homeostasis. On the other side, pathological angiogenesis can be initiated due to the deregulation of inflammatory processes, which results into chronic inflammation [53]. During inflammation, a strong interaction between immune and endothelial cells occurs, and several studies demonstrated that immune/endothelial cell connections encourage cancer development [54]. In the tumor microenvironment, cancer cells release and activate several growth factors, such as VEGF, FGFb, EGF, and TGFb, to promote angiogenesis [55]. Therefore, profiling these factors is critical to comprehend the mechanism underlying angiogenesis. Here, we have profiled 8 angiogenesis cytokines: VEGF, TNF-α, IGF-1, IL-6, FGFb, TGFb, EGF, and leptin; however, only significant deregulation of IL-6 and of FGFb was found after ApoE-Nut-PNPs + US treatment. In the literature, the inhibition of IL-6 expression upon nutlin-3 treatment is reported in several studies [56–58]. In addition, Seki *et al.* showed that IL-6 inhibition leads to reduced anti-angiogenic activity in co-cultures of ovarian clear cell carcinoma (OCCC) cells and HUVECs by increasing angiopoietin-1 (Ang1) secretion and reducing VEGF expression [59]. It can be considered that IL-6 regulates VEGF synthesis, and thus its anti-angiogenic activity may be indirect. FGFs show pro-angiogenic activity by binding to endothelial cell surface receptors such as integrins, tyrosine kinase receptors, and heparan sulfate proteoglycans [60]. Since there is a strong connection between FGFs and angiogenesis [61], the reduction of FGFs levels is considered promising for inhibiting tumor development [62,63]. Among the FGFs, FGFb is one of the well-known pro-angiogenic factors [64], and in this study, we showed a significant reduction of FGFb levels after ApoE-Nut-PNPs + US stimulation. Although the literature reports that electric stimulation enhances angiogenesis in HUVECs by stimulating FGF2 secretion [65], our findings show as the FGFb levels decreased upon ApoE-Nut-PNPs + US administration. This could be potentially ascribable to the fact that nutlin-3 was proven to decrease the expression of *FGF1* following downregulation of p53 [66]; however, further investigations are still required.

5. Conclusion

In the present study, we prepared nutlin-3a-loaded, ApoE-functionalized, and remotely controlled piezoelectric nanoparticles exploited to inhibit tumor-induced angiogenesis. Our results showed that ApoE-Nut-PNPs have an *in vitro* anti-angiogenic activity by inhibiting critical steps in angiogenesis, including vessel formation, endothelial cells migration and invasion, and angiogenesis-related cytokines production. Moreover, the prepared piezoelectric nanovectors enhance the therapeutic efficacy of free drug after US stimulation. Altogether, our study opens a new avenue of using piezoelectric nanoparticles as feasible therapeutics to inhibit angiogenesis, encouraging further investigations towards clinical practice.

Data availability statement

The data that support the findings of this study are available from the authors upon reasonable request.

Author contributions

Özlem Şen: Conceptualization; Investigation; Methodology; Writing – original draft. Attilio Marino: Investigation; Methodology; Data curation; Formal analysis. Carlotta Pucci: Investigation; Methodology; Data curation; Formal analysis. Gianni Ciofani: Conceptualization; Funding acquisition; Project administration; Writing – review & editing.

Declaration of competing interest

The authors declare that they have no known competing financial interests or personal relationships that could have appeared to influence the work reported in this paper.

Acknowledgements

The authors acknowledge the financial support of the European Research Council (ERC) under the European Union's Horizon 2020 research and innovation program (grant agreement 709613, SLaMM). The authors would like moreover to thank Dr. Nerea Iturrioz-Rodríguez (Istituto Italiano di Tecnologia, Italy) for her help in blood sample collection.

Appendix A. Supplementary data

Supplementary data to this article can be found online at https://doi.org/10.1016/j.mtbio.2021.100196.

References

[1] B.A. Saeed, V. Lim, N.A. Yusof, K.Z. Khor, H.S. Rahman, N. Abdul Samad, Antiangiogenic properties of nanoparticles: a systematic review, Int. J. Nanomed. 14 (2019) 5135–5146, https://doi.org/10.2147/IJN.S199974.

[2] Ö. Şen, M. Emanet, G. Ciofani, Nanotechnology-based strategies to evaluate and counteract cancer metastasis and neoangiogenesis, Adv. Healthc. Mater. (2021) 2002163.

[3] R. Lugano, M. Ramachandran, A. Dimberg, Tumor angiogenesis: causes, consequences, challenges and opportunities, Cell. Mol. Life Sci. 77 (2020) 1745–1770.

[4] F. Lopes-Coelho, F. Martins, S.A. Pereira, J. Serpa, Anti-angiogenic therapy: current challenges and future perspectives, Int. J. Mol. Sci. 22 (2021) 3765.

[5] A.M.E. Abdalla, L. Xiao, M.W. Ullah, M. Yu, C. Ouyang, G. Yang, Current challenges of cancer anti-angiogenic therapy and the promise of nanotherapeutics, Theranostics 8 (2018) 533–548, https://doi.org/10.7150/thno.21674.

[6] R.I. Teleanu, C. Chircov, A.M. Grumezescu, D.M. Teleanu, Tumor angiogenesis and anti-angiogenic strategies for cancer treatment, J. Clin. Med. 9 (2020) 84.

[7] H.O. Alsaab, A.S. Al-Hibs, R. Alzhrani, K.K. Alrabighi, A. Alqathama, A. Alwithenani, A.H. Almalki, Y.S. Althobaiti, Nanomaterials for antiangiogenic therapies for cancer: a promising tool for personalized medicine, Int. J. Mol. Sci. 22 (2021) 1631, https://doi.org/10.3390/ijms22041631.

[8] L. Racca, V. Cauda, Remotely activated nanoparticles for anticancer therapy, Nano-Micro Lett. 13 (2021) 1–34.

[9] Y. Jin, N. Chen, Y. Li, Q. Wang, The selective laser sintering of a polyamide 11/BaTiO 3/graphene ternary piezoelectric nanocomposite, RSC Adv. 10 (2020) 20405–20413.

[10] A. Marino, M. Battaglini, D. De Pasquale, A. Degl'Innocenti, G. Ciofani, Ultrasound-activated piezoelectric nanoparticles inhibit proliferation of breast cancer cells, Sci. Rep. 8 (2018) 1–13.

[11] K. Kapat, Q.T.H. Shubhra, M. Zhou, S. Leeuwenburgh, Piezoelectric nano-biomaterials for biomedicine and tissue regeneration, Adv. Funct. Mater. 30 (2020) 1909045.

[12] W. Zhang, J. Wang, P. Gao, S. Tan, W. Zhu, Z. Zhang, Synthesis of poly (vinylidene fluoride–trifluoroethylene) via a controlled silyl radical reduction of poly (vinylidene fluoride–chlorotrifluoroethylene), J. Mater. Chem. C. 5 (2017) 6433–6441.

[13] G.G. Genchi, L. Ceseracciu, A. Marino, M. Labardi, S. Marras, F. Pignatelli, L. Bruschini, V. Mattoli, G. Ciofani, P (VDF-TrFE)/BaTiO3 nanoparticle composite films mediate piezoelectric stimulation and promote differentiation of SH-SY5Y neuroblastoma cells, Adv. Healthc. Mater. 5 (2016) 1808–1820.

[14] T. Jariwala, G. Ico, Y. Tai, H. Park, N.V. Myung, J. Nam, Mechano-Responsive piezoelectric nanofiber as an on-demand drug delivery vehicle, ACS Appl. Bio Mater. 4 (2021) 3706–3715.

[15] C. Pucci, A. Marino, Ö. Şen, D. De Pasquale, M. Bartolucci, N. Iturrioz-Rodríguez, N. di Leo, G. de Vito, D. Debellis, A. Petretto, G. Ciofani, Ultrasound-responsive nutlin-loaded nanoparticles for combined chemotherapy and piezoelectric treatment of glioblastoma cells, Acta Biomater. (2021), https://doi.org/10.1016/j.actbio.2021.04.005.

[16] C. Deben, L.F. Boullosa, A. Domen, A. Wouters, B. Cuypers, K. Laukens, F. Lardon, P. Pauwels, Characterization of acquired nutlin-3 resistant non-small cell lung cancer cells, Cancer Drug Resist 4 (2021) 233–243.

[17] J. Xiong, Q. Yang, J. Li, S. Zhou, Effects of MDM2 inhibitors on vascular endothelial growth factor-mediated tumor angiogenesis in human breast cancer, Angiogenesis 17 (2014) 37–50.

[18] L. Yue, J.-T. Bian, I. Grizelj, A. Cavka, S.A. Phillips, A. Makino, T. Mazzone, Apolipoprotein E enhances endothelial-NO production by modulating caveolin 1 interaction with endothelial NO synthase, Hypertension (Dallas) 60 (2012) (1979) 1040–1046, https://doi.org/10.1161/HYPERTENSIONAHA.112.196667. Dallas, Tex.

[19] B. Weksler, I.A. Romero, P.-O. Couraud, The hCMEC/D3 cell line as a model of the human blood brain barrier, Fluids Barriers CNS 10 (2013) 1–10.

[20] M. J L, D. S, S. Rm, S.T. J, O. S, C.F. van N, H. We, Insights into maleimide-thiol conjugation chemistry: conditions for efficient surface functionalization of nanoparticles for receptor targeting, J. Contr. Release 282 (2018) 101–109, https://doi.org/10.1016/J.JCONREL.2018.03.002.

[21] S. Lu, R. Duffin, C. Poland, P. Daly, F. Murphy, E. Drost, W. Macnee, V. Stone, K. Donaldson, Efficacy of simple short-term in vitro assays for predicting the potential of metal oxide nanoparticles to cause pulmonary inflammation, Environ. Health Perspect. 117 (2009) 241–247, https://doi.org/10.1289/ehp.11811.

[22] A. Marino, E. Almici, S. Migliorin, C. Tapeinos, M. Battaglini, V. Cappello, M. Marchetti, G. De Vito, R. Cicchi, F.S. Pavone, Piezoelectric barium titanate nanostimulators for the treatment of glioblastoma multiforme, J. Colloid Interface Sci. 538 (2019) 449–461.

[23] G. Carpentier, S. Berndt, S. Ferratge, W. Rasband, M. Cuendet, G. Uzan, P. Albanese, Angiogenesis Analyzer for imageJ—a comparative morphometric analysis of "endothelial tube formation Assay" and "fibrin Bead Assay, Sci. Rep. 10 (2020) 1–13.

[24] M.I. Setyawati, D.T. Leong, Mesoporous silica nanoparticles as an antitumoral-angiogenesis strategy, ACS Appl. Mater. Interfaces 9 (2017) 6690–6703.

[25] M.S. Bannon, A. López Ruiz, K. Corrotea Reyes, M. Marquez, Z. Wallizadeh, M. Savarmand, C.A. LaPres, J. Lahann, K. McEnnis, Nanoparticle tracking analysis of polymer nanoparticles in blood plasma, Part. Part. Syst. Char. (2021) 2100016.

[26] I. Zuazo-Gaztelu, O. Casanovas, Unraveling the role of angiogenesis in cancer ecosystems, Front. Oncol. 8 (2018) 248.

[27] N. Hashemi Goradel, F. Ghiyami-Hour, S. Jahangiri, B. Negahdari, A. Sahebkar, A. Masoudifar, H. Mirzaei, Nanoparticles as new tools for inhibition of cancer angiogenesis, J. Cell. Physiol. 233 (2018) 2902–2910.

[28] D. Banerjee, R. Harfouche, S. Sengupta, Nanotechnology-mediated targeting of tumor angiogenesis, Vasc. Cell 3 (2011) 3, https://doi.org/10.1186/2045-824X-3-3.

[29] D. Montizaan, K. Yang, C. Reker-Smit, A. Salvati, Comparison of the uptake mechanisms of zwitterionic and negatively charged liposomes by HeLa cells, Nanomed. Nanotechnol. Biol. Med. 30 (2020) 102300, https://doi.org/10.1016/j.nano.2020.102300.

[30] F. Re, I. Cambianica, S. Sesana, E. Salvati, A. Cagnotto, M. Salmona, P.-O. Couraud, S.M. Moghimi, M. Masserini, G. Sancini, Functionalization with ApoE-derived peptides enhances the interaction with brain capillary endothelial cells of nanoliposomes binding amyloid-beta peptide, J. Biotechnol. 156 (2011) 341–346.

[31] B. Dehouck, L. Fenart, M.-P. Dehouck, A. Pierce, G. Torpier, R. Cecchelli, A new function for the LDL receptor: transcytosis of LDL across the blood–brain barrier, J. Cell Biol. 138 (1997) 877–889.

[32] F. Re, I. Cambianica, C. Zona, S. Sesana, M. Gregori, R. Rigolio, B. La Ferla, F. Nicotra, G. Forloni, A. Cagnotto, M. Salmona, M. Masserini, G. Sancini, Functionalization of liposomes with ApoE-derived peptides at different density affects cellular uptake and drug transport across a blood-brain barrier model, Nanomed. Nanotechnol. Biol. Med. 7 (2011) 551–559, https://doi.org/https://doi.org/10.1016/j.nano.2011.05.004.

[33] A.R. Neves, J.F. Queiroz, S.A.C. Lima, S. Reis, Apo E-functionalization of solid lipid nanoparticles enhances brain drug delivery: uptake mechanism and transport pathways, Bioconjugate Chem. 28 (2017) 995–1004.

[34] N. Hartl, F. Adams, O.M. Merkel, From adsorption to covalent bonding: apolipoprotein E functionalization of polymeric nanoparticles for drug delivery across the blood–brain barrier, Adv. Ther. 4 (2021) 2000092, https://doi.org/10.1002/ADTP.202000092.

[35] F. Hillen, A.W. Griffioen, Tumour vascularization: sprouting angiogenesis and beyond, Cancer Metastasis, Rev 26 (2007) 489–502, https://doi.org/10.1007/s10555-007-9094-7.

[36] A.K. Ferreira, V.M. Freitas, D. Levy, J.L.M. Ruiz, S.P. Bydlowski, R.E.G. Rici, O.M.R. Filho, G.O. Chierice, D.A. Maria, Anti-angiogenic and anti-metastatic activity of synthetic phosphoethanolamine, PLoS One 8 (2013), e57937.

[37] S.H. Chavala, Y. Kim, L. Tudisco, V. Cicatiello, T. Milde, N. Kerur, N. Claros, S. Yanni, V.H. Guaiquil, W.W. Hauswirth, Retinal angiogenesis suppression through small molecule activation of p53, J. Clin. Invest. 123 (2013) 4170–4181.

[38] P. Secchiero, F. Corallini, A. Gonelli, R. Dell'Eva, M. Vitale, S. Capitani, A. Albini, G. Zauli, Antiangiogenic activity of the MDM2 antagonist nutlin-3, Circ. Res. 100 (2007) 61–69.

[39] Z. Su, T. Xu, Y. Wang, X. Guo, J. Tu, D. Zhang, X. Kong, Y. Sheng, W. Sun, Low-intensity pulsed ultrasound promotes apoptosis and inhibits angiogenesis via p38 signaling-mediated endoplasmic reticulum stress in human endothelial cells, Mol. Med. Rep. 19 (2019) 4645–4654, https://doi.org/10.3892/mmr.2019.10136.

[40] D. Janigro, C. Perju, V. Fazio, K. Hallene, G. Dini, M.K. Agarwal, L. Cucullo, Alternating current electrical stimulation enhanced chemotherapy: a novel strategy to bypass multidrug resistance in tumor cells, BMC Cancer 6 (2006) 72, https://doi.org/10.1186/1471-2407-6-72.

[41] G.J. Lim, S.-J. Kang, J.Y. Lee, Novel invasion indices quantify the feed-forward facilitation of tumor invasion by macrophages, Sci. Rep. 10 (2020) 1–10.

[42] L.N. Kiseleva, A.V. Kartashev, N.L. Vartanyan, A.A. Pinevich, M.P. Samoilovich, A172 and T98G cell lines characteristics, Cell tissue Biol. 10 (2016) 341–348.

[43] T. Venkatesan, A. Alaseem, A. Chinnaiyan, S. Dhandayuthapani, T. Kanagasabai, K. Alhazzani, P. Dondapati, S. Alobid, U. Natarajan, R. Schwartz, MDM2 Overexpression modulates the angiogenesis-related gene expression profile of prostate cancer cells, Cells 7 (2018) 41.

[44] S. Delle Monache, A. Angelucci, P. Sanità, R. Iorio, F. Bennato, F. Mancini, G. Gualtieri, R.C. Colonna, Inhibition of angiogenesis mediated by extremely low-frequency magnetic fields (ELF-MFs), PLoS One 8 (2013), e79309.

[45] J. Winkler, A. Abisoye-Ogunniyan, K.J. Metcalf, Z. Werb, Concepts of extracellular matrix remodelling in tumour progression and metastasis, Nat. Commun. 11 (2020) 1–19.

[46] C. Walker, E. Mojares, A. Del Río Hernández, Role of extracellular matrix in development and cancer progression, Int. J. Mol. Sci. 19 (2018) 3028, https://doi.org/10.3390/ijms19103028.

[47] N.V. Krakhmal, M.V. Zavyalova, E.V. Denisov, S.V. Vtorushin, V.M. Perelmuter, Cancer invasion: patterns and mechanisms, Acta Naturae 7 (2015) 17–28. https://pubmed.ncbi.nlm.nih.gov/26085941.

[48] J. Ma, Y. Xue, W. Cui, Y. Li, Q. Zhao, W. Ye, J. Zheng, Y. Cheng, Y. Ma, S. Li, Ras homolog gene family, member A promotes p53 degradation and vascular endothelial growth factor-dependent angiogenesis through an interaction with murine double minute 2 under hypoxic conditions, Cancer 118 (2012) 4105–4116.

[49] Q. Wu, X. Wang, J. Liu, J. Zheng, Y. Liu, Y. Li, F. Su, W. Ou, R. Wang, Nutlin-3 reverses the epithelial-mesenchymal transition in gemcitabine-resistant hepatocellular carcinoma cells, Oncol. Rep. 36 (2016) 1325–1332.

[50] A.C. Weitz, N.S. Lee, C.W. Yoon, A. Bonyad, K.S. Goo, S. Kim, S. Moon, H. Jung, Q. Zhou, R.H. Chow, Functional assay of cancer cell invasion potential based on mechanotransduction of focused ultrasound, Front. Oncol. 7 (2017) 161.

[51] J.Y. Hwang, N.S. Lee, C. Lee, K.H. Lam, H.H. Kim, J. Woo, M.-Y. Lin, K. Kisler, H. Choi, Q. Zhou, R.H. Chow, K.K. Shung, Investigating contactless high frequency ultrasound microbeam stimulation for determination of invasion potential of breast cancer cells, Biotechnol. Bioeng. 110 (2013) 2697–2705, https://doi.org/10.1002/bit.24923.

[52] E.H. Kim, H.S. Song, S.H. Yoo, M. Yoon, Tumor treating fields inhibit glioblastoma cell migration, invasion and angiogenesis, Oncotarget 7 (2016) 65125–65136, https://doi.org/10.18632/oncotarget.11372.
[53] P. Carmeliet, R.K. Jain, Molecular mechanisms and clinical applications of angiogenesis, Nature 473 (2011) 298–307.
[54] D. Aguilar-Cazares, R. Chavez-Dominguez, A. Carlos-Reyes, C. Lopez-Camarillo, O.N. Hernadez de la Cruz, J.S. Lopez-Gonzalez, Contribution of angiogenesis to inflammation and cancer, Front. Oncol. 9 (2019) 1399.
[55] V. Loizzi, V. Del Vecchio, G. Gargano, M. De Liso, A. Kardashi, E. Naglieri, L. Resta, E. Cicinelli, G. Cormio, Biological pathways involved in tumor angiogenesis and bevacizumab based anti-angiogenic therapy with special references to ovarian cancer, Int. J. Mol. Sci. 18 (2017) 1967, https://doi.org/10.3390/ijms18091967.
[56] Y. Fan, W. Zhang, A. Ni, B. Mahato, S.H. Chavala, Inhibition of noncanonical murine double minute 2 homolog abrogates ocular inflammation through NF-κB suppression, Am. J. Pathol. 188 (2018) 2087–2096.
[57] T. Zhang, H. Li, J. Shi, S. Li, M. Li, L. Zhang, L. Zheng, D. Zheng, F. Tang, X. Zhang, F. Zhang, X. You, p53 predominantly regulates IL-6 production and suppresses synovial inflammation in fibroblast-like synoviocytes and adjuvant-induced arthritis, Arthritis Res. Ther. 18 (2016) 271, https://doi.org/10.1186/s13075-016-1161-4.
[58] J.M. Lowe, D. Menendez, P.R. Bushel, M. Shatz, E.L. Kirk, M.A. Troester, S. Garantziotis, M.B. Fessler, M.A. Resnick, p53 and NF-κB coregulate proinflammatory gene responses in human macrophages, Cancer Res. 74 (2014) 2182–2192.
[59] T. Seki, N. Yanaihara, J.S. Shapiro, M. Saito, J. Tabata, R. Yokomizo, D. Noguchi, T. Kuroda, A. Kawabata, J. Suzuki, Interleukin-6 as an enhancer of anti-angiogenic therapy for ovarian clear cell carcinoma, Sci. Rep. 11 (2021) 1–9.
[60] M. Presta, P. Dell'Era, S. Mitola, E. Moroni, R. Ronca, M. Rusnati, Fibroblast growth factor/fibroblast growth factor receptor system in angiogenesis, Cytokine Growth Factor Rev. 16 (2005) 159–178.
[61] J.S. Esser, S. Rahner, M. Deckler, C. Bode, C. Patterson, M. Moser, Fibroblast growth factor signaling pathway in endothelial cells is activated by BMPER to promote angiogenesis, Arterioscler, Thromb. Vasc. Biol. 35 (2015) 358–367.
[62] A. Giacomini, P. Chiodelli, S. Matarazzo, M. Rusnati, M. Presta, R. Ronca, Blocking the FGF/FGFR system as a□ two-compartment□ antiangiogenic/antitumor approach in cancer therapy, Pharmacol. Res. 107 (2016) 172–185.
[63] G. Liu, T. Chen, Z. Ding, Y. Wang, Y. Wei, X. Wei, Inhibition of FGF-FGFR and VEGF-VEGFR signalling in cancer treatment, Cell Prolif 54 (2021), e13009.
[64] F.T. Zahra, M.S. Sajib, C.M. Mikelis, Role of bFGF in acquired resistance upon anti-VEGF therapy in cancer, Cancers 13 (2021) 1422, https://doi.org/10.3390/cancers13061422.
[65] K. Geng, J. Wang, P. Liu, X. Tian, H. Liu, X. Wang, C. Hu, H. Yan, Electrical stimulation facilitates the angiogenesis of human umbilical vein endothelial cells through MAPK/ERK signaling pathway by stimulating FGF2 secretion, Am. J. Physiol. Physiol. 317 (2019) C277–C286.
[66] M. Saison-Ridinger, K.E. DelGiorno, T. Zhang, A. Kraus, R. French, D. Jaquish, C. Tsui, G. Erikson, B.T. Spike, M.N. Shokhirev, C. Liddle, R.T. Yu, M. Downes, R.M. Evans, A. Saghatelian, A.M. Lowy, G.M. Wahl, Reprogramming pancreatic stellate cells via p53 activation: a putative target for pancreatic cancer therapy, PLoS One 12 (2017), https://doi.org/10.1371/journal.pone.0189051 e0189051–e0189051.